Journal of Materials Chemistry A

COMMUNICATION

View Article Online
View Journal | View Issue

Cite this: J. Mater. Chem. A, 2014, 2, 7738

Received 18th March 2014
Accepted 3rd April 2014

DOI: 10.1039/c4ta01337a

www.rsc.org/MaterialsA

Sponge-like $NiCo_2O_4/MnO_2$ ultrathin nanoflakes for supercapacitor with high-rate performance and ultra-long cycle life†

Gao Li,‡[a] Wenyao Li,‡[ab] Kaibing Xu,[a] Rujia Zou,*[a] Zhigang Chen[a] and Junqing Hu*[a]

We present a simple strategy for synthesizing sponge-like $NiCo_2O_4/MnO_2$ ultrathin nanoflakes, which exhibit a high specific capacitance of 935 F g^{-1} at 1 A g^{-1}, excellent rate performance (74.9% retention at 50 A g^{-1}), and ultra-long cycling stability (103.1% of the initial capacitance after 25 000 cycles).

Transition metal oxides (TMOs), especially in the form of nanomaterials, had been extensively studied as electrode materials of pseudocapacitors in the past decades.[1–5] This can be interpreted as their abundant Faradaic redox reactions, which contribute to high specific capacitances.[6] However, TMOs with which redox reactions are involved often suffer from a lack of stability during long-term cycling.[7] Furthermore, the low electronic conductivity of TMOs profoundly restricts their rate performance.[8,9] An attractive concept to alleviate the previously mentioned negative effects is to combine two or more types of TMOs. Mixed TMOs as prospective electrode materials, which could inherit advantages from individual TMOs and generate excellent properties, have received an upsurge of interest in recent years. For instance, Xia *et al.*[10] reported the Co_3O_4/NiO core–shell nanowire arrays for pseudocapacitors with an enhanced capacitance (853 F g^{-1} at 2 A g^{-1}), rate performance and electrochemical stability; Liu *et al.*[11] reported the MnO_2/NiO tube arrays for pseudocapacitors with an improved capacitance (0.35 F cm^{-2} at 8.5 mA cm^{-2}) with respect to pristine MnO_2 tubular arrays, a good cycle performance, and remarkable rate capability.

In addition to anticipating composition, the performance of TMOs in various applications also heavily depends on the microtexture of the materials.[12] Therefore, the rational design of electrode materials with well-defined micro/nanostructures is imperative for further enhancement of the electrochemical properties. Hierarchical structures, which draw special interest due to their exceptional properties and remarkable potential in many fields, have been synthesized for many simple metal oxides, but the facile synthesis of the mixed TMOs with desirable composition and hierarchical structure still remains a challenge.[13,14] Thus, it is desired that well-designed compositions for supercapacitors with encouraging electrochemical performance, especially that of high-rate performance and long-term cycling stability, could be synthesized by a facile method.

Based on the previous discussion, we present a simple strategy to fabricate sponge-like $NiCo_2O_4/MnO_2$ ultrathin nanoflakes on graphite paper with remarkable capacitive performance. $NiCo_2O_4$ and MnO_2 are composited into sponge-like ultrathin nanoflakes *via* a simple one-step electrodeposition with subsequent annealing. When applied as an electrode, the smartly designed composites possess three merits: (I) ultrathin nanoflakes would enable a fast, reversible Faradaic reaction and provide a short ion diffusion path, hence a good rate performance can be obtained;[15] (II) the fluffy, sponge-like structure is advantageous to the permeation of the electrolyte to the inner electrode, as well as the emission of joule heat to the electrolyte, thus increasing the thermal stability of the structure;[16,17] and (III) ultrathin nanoflakes are strongly supported on graphite paper, in which binding and conductive additives can be avoided and, consequently, the inactive surface is significantly reduced.[18] The electrochemical measurements show that the specific capacitance of the sponge-like $NiCo_2O_4/MnO_2$ ultrathin nanoflakes achieves a maximum of 935 F g^{-1} at a current density of 1 A g^{-1}, which could still retain 700 F g^{-1} (74.9% retention) even if the current density reaches as high as 50 A g^{-1}. Moreover, the electrode maintains 103.1% capacitance of initialization after 25 000 cycles, illustrating ultra-long cycling stability. These results show that the sponge-like $NiCo_2O_4/MnO_2$ ultrathin nanoflakes should be a very promising electrode material for supercapacitors.

[a]State Key Laboratory for Modification of Chemical Fibers and Polymer Materials, College of Materials Science and Engineering, Donghua University, Shanghai 201620, China. E-mail: rjzou@dhu.edu.cn; hu.junqing@dhu.edu.cn; Fax: +86-021-6779-2947; Tel: +86-021-6779-2947

[b]School of material engineering, Shanghai university of engineering science, Shanghai 201620, China

† Electronic supplementary information (ESI) available. See DOI: 10.1039/c4ta01337a

‡ These authors contributed equally to the work.

Fig. 1a shows the X-ray diffraction (XRD) pattern of the $NiCo_2O_4/MnO_2$ ultrathin nanoflakes. As observed in Fig. 1a, except for the two strong peaks from the graphite paper substrate, other well-defined diffraction peaks confirm the existence of the spinel $NiCo_2O_4$ phase (JCPDS card no. 20-0781). The peak at 12.9° comes from the tetragonal MnO_2 phase (JCPDS card no. 44-0141). The chemical composition of the sample was further analyzed by X-ray photoelectron spectroscopy (XPS) shown in Fig. S1 (ESI†). High-resolution XPS spectra of Mn 2p, Co 2p and Ni 2p for the $NiCo_2O_4/MnO_2$ ultrathin nanoflakes are presented in Fig. 1b–d. By using a Gaussian fitting method, Fig. 1b of the Mn 2p region demonstrates two main peaks at 642.4 and 653.7 eV, indicating that the elemental Mn is in the formation of MnO_2.[11,19,20] The Co 2p spectrum (Fig. 1c) is best fitted considering the two spin–orbit doublets characteristic of Co^{2+} and Co^{3+} and one shakeup satellite (identified as "Sat."). The Ni 2p spectrum (Fig. 1d) is best fitted considering the two spin–orbit doublets characteristic of Ni^{2+} and Ni^{3+} and two shakeup satellites. These results show that the $NiCo_2O_4/MnO_2$ ultrathin nanoflakes have a composition containing Co^{2+}, Co^{3+}, Ni^{2+} and Ni^{3+}, which is in good agreement with literature for $NiCo_2O_4$.[18,21] Additionally, the uniform distribution of Mn, Ni and Co species is confirmed by the line-scan mapping (Fig. S2, see ESI†), which reveals that the composition is mainly composed of $NiCo_2O_4$ and only contains a few of the MnO_2.

Low- and high-magnification field emission scanning electron microscopy (FESEM) images of the sample are shown in Fig. 2. A low FESEM image viewed from the top can be seen in Fig. 2a, which indicates that the entire material on the graphite paper is homogeneous. A high-magnification image of the sample is shown in Fig. 2b, which reveals that the architecture is composed of numerous ultrathin nanoflakes (<10 nm) and has a cross-linked character, in which channels and pores are formed. Low- and high-magnification FESEM images of the cross section are available in Fig. 2c and d, respectively. Fig. 2c reveals that the thickness of the architecture is ~2 μm. Fig 2d elucidates that the ultrathin nanoflakes are standing over the graphite paper; thus, it is beneficial to the charge transport and ion diffusion without the necessity of binder blocks, which results in improved charge transfer kinetics. Notably, the cross-linked ultrathin nanoflakes provide a fluffy, sponge-like architecture to facilitate the permeation of the electrolyte to the inner electrode, as well as the emission of joule heat to the electrolyte.

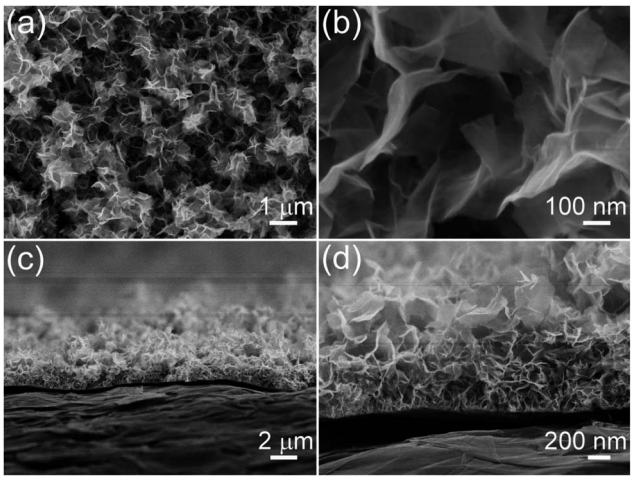

Fig. 2 (a) Low- and (b) high-magnification FESEM images from the top view, and (c) low- and (d) high-magnification FESEM images of the side view.

To better understand the structure, representative transmission electron microscopy (TEM) images taken from the sample are given in Fig. 3a and b. The dark strips in Fig. 3a are generally the folded edges or wrinkles of the nanoflakes. The magnified images of Fig. 3b clearly show that mesopores are uniformly distributed throughout the entire surface of the nanoflakes. The sizes of the mesopores are estimated to be in the range of 2–5 nm. It is well known that the mesoporous structures in nanoflakes facilitate the mass transport of electrodes within

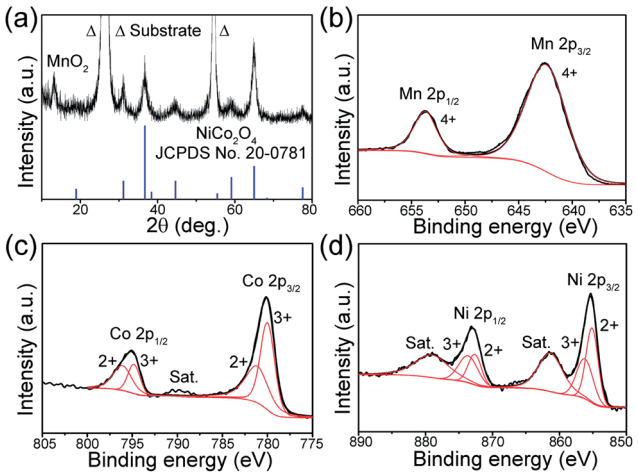

Fig. 1 (a) XRD pattern of the $NiCo_2O_4/MnO_2$ ultrathin nanoflakes. (b) Mn 2p, (c) Co 2p and (d) Ni 2p spectra of the $NiCo_2O_4/MnO_2$ ultrathin nanoflakes.

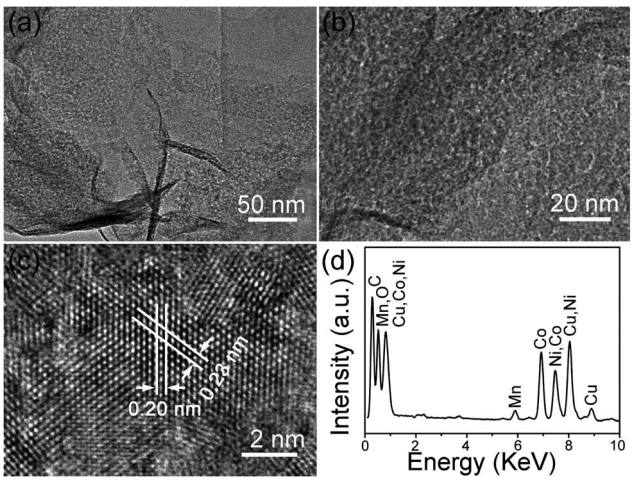

Fig. 3 (a) Low-magnification TEM image. (b) Enlarged TEM image. (c) HRTEM image of $NiCo_2O_4/MnO_2$ ultrathin nanoflakes. (d) EDX pattern taken from ultrathin nanoflakes.

electrolytes for Faradaic redox reactions.[7,22] The mesoporous structure will also enlarge the electrode/electrolyte contact areas, which further enhances the electrochemical performance of electrode.[12] As can be seen from the HRTEM image of Fig. 3c, the lattice fringes give an interplanar spacing of 0.23 nm and 0.20 nm, corresponding to that of the {222} and {400} lattice planes of the spinel $NiCo_2O_4$ crystal, respectively. The EDX spectrum is shown in Fig. 3d. The presence of Mn, Co and Ni is in agreement with our designed concept, and the Cu and C signals clearly come from the TEM grid.

The electrochemical measurements were performed on an Autolab (PGSTAT302N) with a three-electrode configuration system in 1 M KOH aqueous solution within the potential window of −0.1 to 0.5 V (*vs.* Ag/AgCl) to evaluate the electrochemical performance of the as-synthesized electrodes. The samples vary according to the electrodeposition time, particularly 20, 30 and 40 min (denoted as P1, P2 and P3, respectively). The specific capacitance values of the samples had been determined by cyclic voltammetry (CV) and galvanostatic charge–discharge (CD) measurements. Fig. 4a shows the CV curves of the P1 sample at different scan rates. Strong redox peaks over the entire range of scan rates can be clearly observed, which reveals that the capacitive characteristics are mainly governed by the Faradaic reaction. It is notable that the capacitance contributed from the graphite paper substrate is negligible (Fig. S3, ESI†).

It is well accepted that galvanostatic charge–discharge examination is an established method for estimating specific capacitance. Fig. 4b presents the typical charge–discharge voltage *vs.* the time plots of the P1 sample at various current densities. A symmetric nonlinear triangular shape is observed, further indicating their pseudo-capacitance behavior and excellent reversibility. The specific capacitance of the P1 sample at various current densities can be calculated based on the corresponding CD curves, and the results are depicted in Fig. 4c together with the other two samples. The P1 sample manifests high specific capacitance values of 935, 923, 895, 863, 813, 770, 740 and 700 F g^{-1} at current densities of 1, 2, 5, 10, 20, 30, 40 and 50 A g^{-1}, respectively, which is superior to the other two samples (Table S1 in ESI†). This is mainly due to that as for the P2 and the P3 sample, a dense layer (Fig. S4, ESI†) covering on the sponge-like ultrathin nanoflakes prevents the electrolyte from permeating into the sponge-like ultrathin nanoflakes, and only the outer surface of the dense layer can be utilized for the charge storage. It can be deduced that the thickness of the dense layer should increase as electrodeposition time goes on, and then specific capacitance values would decrease. The CD curves of the P2 and the P3 sample are shown in Fig. S5a and b (ESI†) for further demonstration. All of these samples simultaneously show high rate capabilities (74.9% for P1, 81.8% for P2, and 53.7% for P3) when current densities increase from 1 to 50 A g^{-1}, which can be ascribed to that ultrathin nanoflakes enable a fast Faradaic reaction and provide a short ion diffusion path.

Cycling stability is another critical factor in evaluating the electrochemical properties of supercapacitors. The cycling stability curves of the three electrodes at a scan rate of 50 mV s^{-1} are illustrated in Fig 4d. The final specific capacitance of the P1 sample retained 103.1% of its initial value when it had undergone 25 000 cycles. In other words, the loss in specific capacitance based on the maximum value is only ~8.7%. Such an ultralong cycle life that can be ascribed to the fluffy sponge-like structure is advantageous to the emission of joule heat to the electrolyte, hence increasing the thermal stability of the structure. However, cycling performances of the P2 (87.8% retention) and P3 (71.1% retention) samples are slightly satisfactory. It can be attributed to the denser layers of the P2 and P3 samples, which cannot adapt well to the pronounced volume expansion/contraction and result in the pulverization of the electrode material. The Nyquist plots of the P1 sample are also presented in Fig. 4e. It is known that the equivalent series resistance (ESR) is an important characteristic of supercapacitors measured at high-frequency regions where the curve intersects on the real axis. The higher ESR indicates the lower electrical conductivity of the sample. It can be seen that the P1 sample shows ESR value ~2.7 Ω before cycling. After 25 000 cycles, the P1 sample exhibits lower ESR (~1.3 Ω), which is due to the activation of active material during the cycling process. In addition, after 25 000 cycles, the slope is close to 90° at the low-frequency region, which indicates that the P1 sample has good capacitive behaviour.

In view of the excellent rate capability and ultra-long cycling life, we further calculate the energy and power densities, which are the two key factors for the practical applications of supercapacitors. The results are presented as Ragone plots in Fig. 4f. The P1 sample can deliver high power output in the range of 0.3 and 15 kW kg^{-1} with little sacrifice of the high energy density

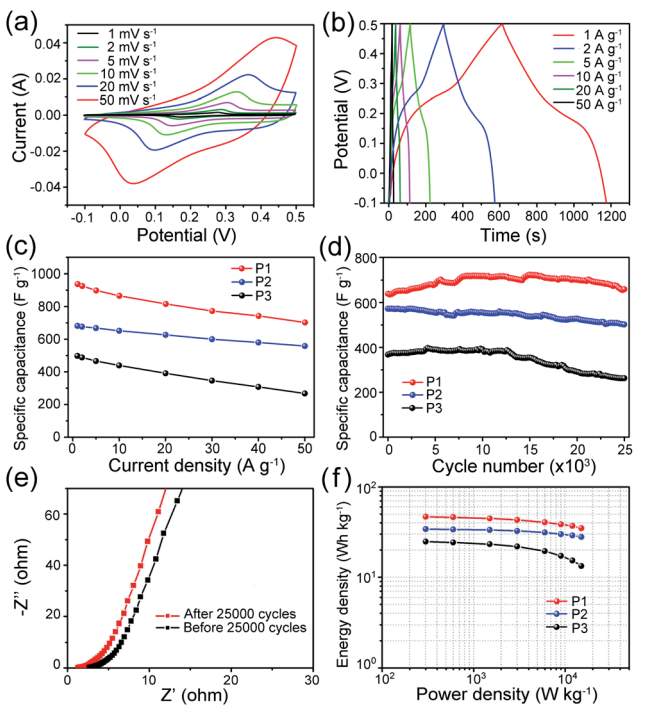

Fig. 4 (a) CV and (b) CD curves of the P1 sample. (c) Specific capacitance as a function of the current of P1, P2 and P3 samples. (d) Cycling performances of P1, P2 and P3 samples at a scan rate of 50 mV s^{-1}. (e) Nyquist plot of the P1 sample. (f) Ragone plots of P1, P2 and P3 samples.

(from 46.75 to 35 W h kg^{-1}), better than that of the P2 (34.1 to 27.9 W h kg^{-1}) and P3 (24.8 to 13.3 W h kg^{-1}) samples. This result further confirms that the sponge-like $NiCo_2O_4/MnO_2$ ultrathin nanoflakes of the P1 sample is an excellent capacitive material.

Based on previous discussions, we have determined that the sponge-like $NiCo_2O_4/MnO_2$ ultrathin nanoflakes of the P1 sample possessed the best electrochemical performance. However, it should be truly understood whether this strategy to synthesize $NiCo_2O_4/MnO_2$ is of any advantage with respect to pure $NiCo_2O_4$ because $NiCo_2O_4$ exhibits good pseudocapacitive behavior.[23–27] The pure $NiCo_2O_4$ was prepared by using the solution without $Mn(NO_3)_2$ under the same conditions. The electrochemical performances of the obtained pure $NiCo_2O_4$ and $NiCo_2O_4/MnO_2$ are shown in Fig. S6 (ESI†). Fig. S6a† shows the cyclic voltammetry (CV) curves of $NiCo_2O_4/MnO_2$ and pure $NiCo_2O_4$ at a scan rate of 10 mV s^{-1}. The specific capacitance of pure $NiCo_2O_4$ is 1005 F g^{-1}, which is higher than that of $NiCo_2O_4/MnO_2$ (839 F g^{-1}). Fig. S6b† shows the galvanostatic charge–discharge (CD) curves of $NiCo_2O_4/MnO_2$ and pure $NiCo_2O_4$ at a current density of 5 A g^{-1}. The specific capacitance of pure $NiCo_2O_4$ calculated from CD curves is larger than that of $NiCo_2O_4/MnO_2$. However, when we focus on the rate performance and cycling stability of the materials, which are also as important as the specific capacitance, we determine that $NiCo_2O_4/MnO_2$ acquired high-rate performance and improved cycling stability than pure $NiCo_2O_4$. Fig. S6c† shows that $NiCo_2O_4/MnO_2$ exhibits a high-rate performance of 74.9% retention, compared with 70.3% retention from pure $NiCo_2O_4$. Fig. S6d† indicates that $NiCo_2O_4/MnO_2$ possesses ultra-long cycling stability (103.1% of the initial capacitance after 25 000 cycles), while pure $NiCo_2O_4$ can only retain 73.6% of its initial capacitance after 15 000 cycles. The excellent rate performance and ultra-long cycling stability of $NiCo_2O_4/MnO_2$ demonstrate that this strategy is advantageous.

In summary, sponge-like $NiCo_2O_4/MnO_2$ ultrathin nanoflakes on graphite paper were synthesized by a simple process of electrodeposition with subsequent annealing. The as-synthesized electrode by 20 min electrodeposition exhibited an enhanced specific capacitance of 935 F g^{-1} at 1 A g^{-1} with high rate performance (74.9% capacity retention at 50 A g^{-1}) and ultra-long cycling stability (maintaining 103.1% capacitance of initialization after 25 000 cycles), which make the sponge-like $NiCo_2O_4/MnO_2$ ultrathin nanoflakes a promising electrode material for high-performance supercapacitors.

Acknowledgements

This work was financially supported by the National Natural Science Foundation of China (Grant Nos. 21171035 and 51302035), the Key Grant Project of Chinese Ministry of Education (Grant No. 313015), the PhD Programs Foundation of the Ministry of Education of China (Grant Nos. 20110075110008 and 20130075120001), the National 863 Program of China (Grant No. 2013AA031903), the Science and Technology Commission of Shanghai Municipality (Grant No. 13ZR1451200), the Program for Changjiang Scholars and Innovative Research Team in University (Grant No. IRT1221), the Hong Kong Scholars Program, the Project funded by China Postdoctoral Science Foundation, the Fundamental Research Funds for the Central Universities, the Shanghai Leading Academic Discipline Project (Grant No. B603), and the Program of Introducing Talents of Discipline to Universities (Grant No. 111-2-04).

Notes and references

1 W. Chen, R. B. Rakhi, L. B. Hu, X. Xie, Y. Cui and H. N. Alshareef, *Nano Lett.*, 2011, **11**, 5165.
2 C. Liu, F. Li, L. P. Ma and H. M. Cheng, *Adv. Mater.*, 2010, **22**, E28.
3 C. Guan, J. Liu, C. Cheng, H. Li, X. Li, W. Zhou, H. Zhang and H. J. Fan, *Energy Environ. Sci.*, 2011, **4**, 4496.
4 R. B. Rakhi, W. Chen, D. Cha and H. N. Alshareef, *Nano Lett.*, 2012, **12**, 2559.
5 C. Yuan, L. Yang, L. Hou, L. Shen, X. Zhang and X. W. Lou, *Energy Environ. Sci.*, 2012, **5**, 7883.
6 J. Jiang, Y. Li, J. Liu, X. Huang, C. Yuan and X. W. Lou, *Adv. Mater.*, 2012, **24**, 5166.
7 P. Simon and Y. Gogotsi, *Nat. Mater.*, 2008, **7**, 845.
8 C. C. Hu, K. H. Chang, M. C. Lin and Y. T. Wu, *Nano Lett.*, 2006, **6**, 2690.
9 Y. B. He, G. R. Li, Z. L. Wang, C. Y. Su and Y. X. Tong, *Energy Environ. Sci.*, 2011, **6**, 5531.
10 X. H. Xia, J. P. Tu, Y. Q. Zhang, X. L. Wang, C. D. Gu, X. B. Zhao and H. J. Fan, *ACS Nano*, 2013, **6**, 5531.
11 J. P. Liu, J. Jiang, M. Bosman and H. J. Fan, *J. Mater. Chem. A*, 2012, **22**, 2419.
12 H. B. Wu, H. Pang and X. W. Lou, *Energy Environ. Sci.*, 2013, **6**, 3619.
13 L. Xiao, Y. Yang, J. Yin, Q. Li and L. Zhang, *J. Power Sources*, 2009, **194**, 1089.
14 Q. Wang, B. Liu, X. Wang, S. Ran, L. Wang, D. Chen and G. Shen, *J. Mater. Chem.*, 2012, **22**, 21647.
15 L. Yu, G. Q. Zhang, C. Z. Yuan and X. W. Lou, *Chem. Commun.*, 2013, **49**, 137.
16 J. Yan, W. Sun, T. Wei, Q. Zhang, Z. Fan and F. Wei, *J. Mater. Chem.*, 2012, **22**, 11494.
17 C. Y. Cao, W. Guo, Z. M. Cui, W. G. Song and W. Cai, *J. Mater. Chem.*, 2011, **21**, 3204.
18 C. Z. Yuan, J. Y. Li, L. R. Hou, X. G. Zhang, L. F. Shen and X. W. Lou, *Adv. Funct. Mater.*, 2012, **22**, 4592.
19 H. W. Nesbitt and D. B. Anerjee, *Am. Mineral.*, 1998, **83**, 305.
20 C. Zhou, H. Wang, F. Peng, J. Liang, H. Yu and J. Yang, *Langmuir*, 2009, **25**, 7711.
21 B. Cui, H. Lin, Y. Z. Liu, J. B. Li, P. Sun, X. C. Zhao and C. J. Liu, *J. Phys. Chem. C*, 2009, **113**, 14083.
22 Z. Wang, L. Zhou and X. W. Lou, *Adv. Mater.*, 2012, **24**, 1903.
23 L. F. Shen, Q. Che, H. S. Li and X. G. Zhang, *Adv. Funct. Mater.*, DOI: 10.1002/adfm.201303138.
24 G. Q. Zhang, H. B. Wu, H. E. Hoster, M. B. Chan-Park and X. W. Lou, *Energy Environ. Sci.*, 2012, **5**, 9453.
25 G. Q. Zhang and X. W. Lou, *Adv. Mater.*, 2013, **25**, 976.
26 W. L. Yang, Z. Gao, J. Ma, X. M. Zhang, J. Wang and J. Y. Liu, *J. Mater. Chem. A*, 2014, **2**, 1448.
27 C. Z. Yuan, J. Y. Li, L. R. Hou, J. D. Lin, X. G. Zhang and S. L. Xiong, *J. Mater. Chem. A*, 2013, **1**, 11145.